AGU PUBLICATIONS

Space Weather

RESEARCH ARTICLE
10.1002/2014SW001129

Key Points:
- Thumba and Sriharikota ionosondes from Indian sector have been utilized
- Investigation on the F layer height rise and ESF onset time has been presented
- Observations highlight the important role of LSWS in ESF

Correspondence to:
L. M. Joshi,
lmjoshinarl@gmail.com

Citation:
Joshi, L. M., S. Balwada, T. K. Pant, and S. G. Sumod (2015), Investigation on *F* layer height rise and equatorial spread *F* onset time: Signature of standing large-scale wave, *Space Weather*, *13*, doi:10.1002/2014SW001129.

Received 2 OCT 2014
Accepted 2 MAR 2015
Accepted article online 6 MAR 2015

Investigation on *F* layer height rise and equatorial spread *F* onset time: Signature of standing large-scale wave

Lalit Mohan Joshi[1], S. Balwada[2], T. K. Pant[3], and S. G. Sumod[4,5]

[1]Indian Institute of Geomagnetism Mumbai, Mumbai, India, [2]National Atmospheric Research Laboratory, Chittoor, India, [3]Vikram Sarabhai Space Centre, ISRO, Thiruvananthapuram, India, [4]Laboratório de Fisica e Astronomia, UNIVAP, São Paulo, Brazil, [5]Department of Physics, Sacred Heart College, Kochi, India

Abstract Equatorial spread *F* observations have been categorized into three categories based on ionograms recorded over Sriharikota. First category comprised cases where the onset of equatorial spread *F* (ESF) was concurrent with the peak *h'F* time. Second and third categories comprised cases where the onset of ESF happened with a delay of 30 min and more than 30 min, respectively, with reference to the peak *h'F* time. Average peak *h'F* in the first category was more than 35 km higher than that in the second and third categories. Also, the peak vertical (upward) plasma drift was higher in the first category. Assuming the genesis of *F* region irregularity to have happened at or before the time of *F* layer attaining the peak height, late onset of ESF indicates the genesis of irregularities to have happened westward of Sriharikota. The fact that the peak *h'F* values were remarkably different in the three categories indicates a zonal variation of eastward electric field and postsunset height rise of *F* layer. The relative magnitude of the *F* layer height rise in the three different categories over Sriharikota has also been found to be significantly different than that over Thumba, an equatorial (magnetic) station located ~360 km westward of Sriharikota longitude. This scenario points toward the existence of a large-scale zonal standing wave in the *F* layer and its important role in *F* region instability process. Results presented in the manuscript have been discussed in the light of current understanding on the large-scale wave structure.

1. Introduction

Day-to-day variability of the equatorial spread F (ESF) continues to be a puzzle even decades after the first scientific investigation was carried out to reveal its existence and behavior. It refers to the unusually large spread in the *F* region echo trace seen on the ionosonde, a swept frequency pulsed radar. It constitutes an important aspect of ionospheric weather and affects satellite based navigation and communication applications. Although we know that the main cause of this enigmatic phenomenon is the generation of the equatorial plasma bubble (EPB), several interesting aspects of it have not been fully understood. One such aspect is the large-scale spatial modulation in its occurrence. Large-scale wave structure (LSWS), originating in the *F* region during the evening hours has been considered to be the main cause of it [*Tsunoda and White*, 1981]. It is being believed that the day-to-day variability of the ESF is controlled by the occurrence and the behavior of the LSWS.

LSWS and its role in the formation of plasma bubble have been studied using a variety of observational tools, which include incoherent scatter radar [*Tsunoda and White*, 1981], ionosonde [*Tsunoda*, 2008, 2009], airglow photometer [*Patra et al*., 2013], and satellite measurement [e.g., *Thampi et al*., 2009; *Huang et al*., 2013]. Investigations carried out so far to study the role of LSWS in the formation of plasma bubble have mostly been in the form of case studies based on limited number of events [e.g., *Tsunoda and White*, 1981; *Tsunoda*, 2008, 2009; *Patra et al*., 2013; *Thampi et al*., 2009; *Huang et al*., 2013; *Tsunoda and Ecklund*, 2007], except the investigation by *Tulasi Ram et al*. [2014a], comprising ~70 days of observations from the African sector and 99 days of observations from the Asian sector. In fact, the actual role and importance of the LSWS in the onset of the ESF can only be ascertained by examining a long-term and continuous data set.

ESF not only remains to be a matter of scientific quest but also poses as a technological challenge in the field of satellite-based navigation and communication [*Shume et al*., 2013; *Bagiya et al*., 2013; *Oladipo et al*., 2014]. Several investigations in the recent times have highlighted the day-to-day variability in the ionospheric

irregularities [e.g., *Whalen*, 2007] and its impact on the satellite-based navigation through L band scintillation [e.g., *de Lima et al*., 2014; *Zhang et al*., 2010; *Sreeja et al*., 2011, 2012; *Aquino and Sreeja*, 2013]. Recently, *Kelly et al*. [2014] have highlighted how ESF can critically hamper real-time UHF communication. Thus, investigations on the causative mechanisms of the ESF are required, also from the technological perspectives. One of the potential causes of the ESF is the LSWS.

One of the most interesting features of the LSWS is the lack of zonal propagation with time [*Tsunoda and Ecklund*, 2007]. LSWS originates as a standing wave of plasma density in the *F* region, gains amplitude with time, and believed to result in the formation of plasma bubbles. This paper deals with the relation of the onset time of the equatorial spread *F* and the peak height attained by the *F* layer in the evening hours. If the postsunset height rise of the *F* layer is purely time dependent, the onset time of spread *F* and the peak height attained by the *F* layer will have no relationship. However, if the postsunset height rise of the *F* layer depends on time as well as the zonal location, spread *F* onset time can be related to the peak height attained by the *F* layer. Later scenario points toward the existence of the LSWS. This aspect has been discussed in details in this paper.

2. Data and Methodology

Ionosonde observations made during 15 February 2004 to 2 April 2004 period (48 days) from Sriharikota (13.7°N, 80.1°E, and 6.7°N magnetic latitude) and Thumba (8.53°N, 76.87°E, and 0.2°N magnetic latitude) in India have been used for the study presented in this paper. KEL IPS-42 digital ionosonde has been used for making the observations. Observations were made once every 15 min. Range resolution of the ionosonde was ~3 km. Observations were recorded digitally and were analyzed using the software supplied by the instrument manufacturer (KEL Aerospace), to derive the standard parameter like *h'F*. Vertical plasma drift of the *F* layer has been inferred by calculating the rate of change of *F* layer height ($V_Z = dh'F/dt$). During the entire observational period, the average $F_{10.7}$ was 110 solar flux unit. Of all the spread *F* nights discussed in this manuscript, two nights belonged to geomagnetically active period (2 and 11 March). A geomagnetic storm has also occurred on 9 March 2004 (refer to *Tulasi Ram et al*. [2008] and *Tulasi Ram et al*. [2014b]). Thus, the observation recorded on the night of 9 March 2004 has been excluded from the analysis presented in this manuscript, so as to focus primarily on the quite time variability of ESF. For detailed study we have divided the spread *F* cases based on ionograms recorded over Sriharikota into three categories: Category 1 (24 February and 6, 8, 19, 23–25, and 27 March), Category 2 (22 and 23 February and 11, 16, and 26 March), and Category 3 (21 February and 5, 13, 14, 20, 22, and 29 March). Basis for this categorization has been mentioned in details in subsequent sections.

3. Results

3.1. Time of *F* Layer Attaining the Peak Height and Spread *F* Onset Time

Zonal electric field is eastward during the day and westward during the night. Prior to its reversal during the evening hours, from eastward to westward, the zonal eastward electric field shows an enhancement. This enhancement of eastward electric field, prior to its reversal to westward, is termed as prereversal enhancement (PRE) of zonal electric field. Magnitude of this enhancement displays a day-to-day, seasonal, and solar cycle variations. This phenomenon has been studied in details, and several mechanisms have been proposed to explain its cause [e.g., *Farley et al*., 1986; *Haerendel and Eccles*, 1992]. Enhancement in the eastward electric field cause the postsunset height rise of the *F* layer. Height of the *F* layer in the postsunset hours rises till the time of zonal electric field turns westward, after which it descends. This height rise plays an important role in the generation of equatorial plasma bubble by enhancing the growth rate of the Rayleigh-Taylor (RT) instability. Also, the eastward electric field enhances the growth of the RT instability. Thus, the genesis of *F* region irregularity is expected to happen either at the time of *F* layer attaining the peak height or before it [*Abdu et al*., 1983; *Sastri et al*., 1997].

Figure 1 presents the distribution of peak *h'F* timing based on Sriharikota ionosonde observations corresponding to those nights when spread *F* has occurred. Out of the total 48 nights of continuous observations, spread *F* occurred on 30 nights (thus, the occurrence of spread *F* was ~62%). The time of *F* layer attaining the peak height varied between 19:00 IST and 20:30 IST. Here IST stands for the Indian Standard Time (UT + 5:30 h), which lags by ~8 min with respect to the local time at Sriharikota. Number of cases where the onset time of ESF coincided with the time of the *F* layer attaining the peak height is shown in green color in the histogram. In most of the nights, peak *h'F* was attained at or before 19:45 IST. In 10 out of 30 cases peak *h'F* was attained at 19:30 IST.

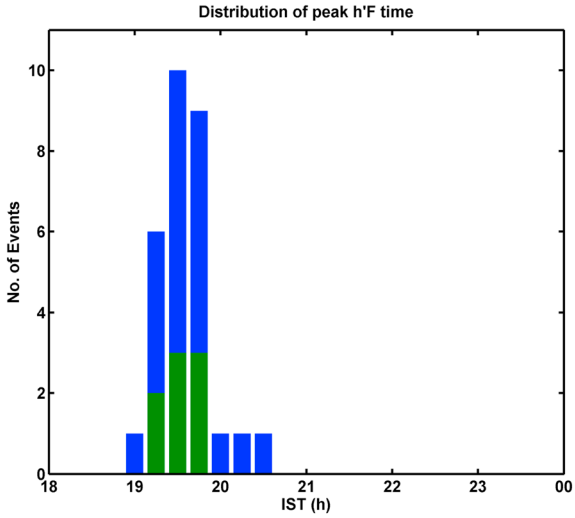

Figure 1. Histogram of the time of *F* layer attaining the peak height (peak *h'F* time), based on the ionosonde observations on spread *F* nights.

Growth of RT instability maximizes at a time when *F* region reaches peak height. Thus, the genesis of *F* region irregularities happens close to the time of *F* layer attaining the peak height. It becomes important to examine the time of spread *F* onset in the ionosonde observations. Figure 2 presents the distribution of the spread *F* onset time. It is interesting to see that distribution of spread *F* onset timing is quite different than that of the *F* layer attaining the peak height. While the peak height was attained by the *F* layer before 19:45 IST in most cases, spread *F* onset in the ionograms were observed after that.

3.2. Height Migration of *F* Layer in Early and Late Spread *F* Onset Cases

As presented earlier in Figures 1 and 2, it is evident that the onset of ESF always did not coincide with the time of *F* layer attaining the peak height. On a few cases onset of spread *F* was observed at the time of *F* layer attaining the peak height. On the other hand, there were cases where the onset of spread *F* was delayed by 15, 30, 45 min or even more than that, with respect to the peak *h'F* time. Height migration of *F* layer has been investigated in details corresponding to three different categories: early spread *F* onset cases, where the onset of spread *F* happened at or before the time of *F* layer attaining the peak height, moderately delayed spread *F* cases, where onset of spread *F* was observed after 30 min of *F* layer attaining the peak height, and late spread *F* onset cases, where the onset of spread *F* was delayed by 45 min or more with respect to the time of *F* layer attaining the peak height. Cases where the onset of spread *F* has been delayed by 15min have not been considered for the detailed analysis. This is because of the fact that the soundings were made every 15 min, and with this sampling rate it will not be possible to really characterize those cases into early or delayed spread *F* onset cases.

Figure 3a presents the *h'F* observed over Sriharikota corresponding to the early spread *F* onset cases. Here blue color line and symbol have been used to indicate the observation of classic *F* layer echo trace. Observation of spread *F* has been indicated by red color line and symbol. Average *h'F* value has been indicated by thick black line. One can see that the transition from blue to red color occurred at the time of *F* layer attaining the peak height (peak *h'F*). Here the peak *h'F* was attained at ~19:30 IST in most cases. Another interesting aspect is the enhanced level of *F* layer height rise. In most cases the peak *h'F* was more than 350 km, while the average peak *h'F* was ~350 km. Vertical plasma drift velocity has also been obtained using the ionosonde measurements. Vertical plasma drifts (V_Z) for the cases discussed above is presented in Figure 3b. Maximum V_Z in all the cases exceeded 20 m s^{-1}, and it became zero around 19:30 IST, indicating the reversal of electric field.

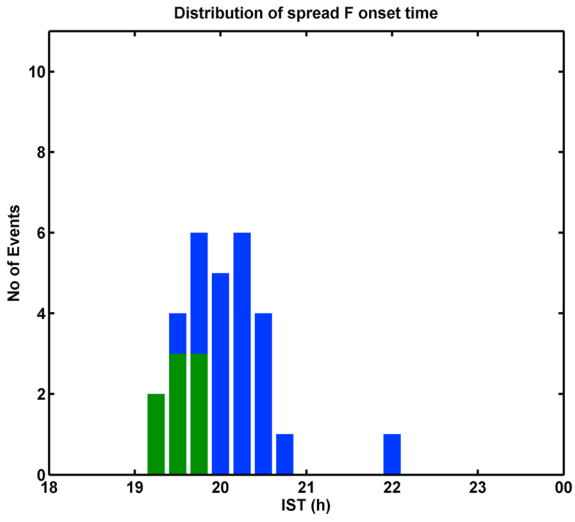

Figure 2. Histogram of the time of onset of ESF recorded in the ionograms.

F layer height variation and the V_Z corresponding to the moderately delayed spread *F* cases are indicated in Figures 3c and 3d, respectively. Peak *h'F* values in this category were in general less than those for the cases discussed in Figure 3a. Also, the peak vertical plasma drifts, V_Z, were in

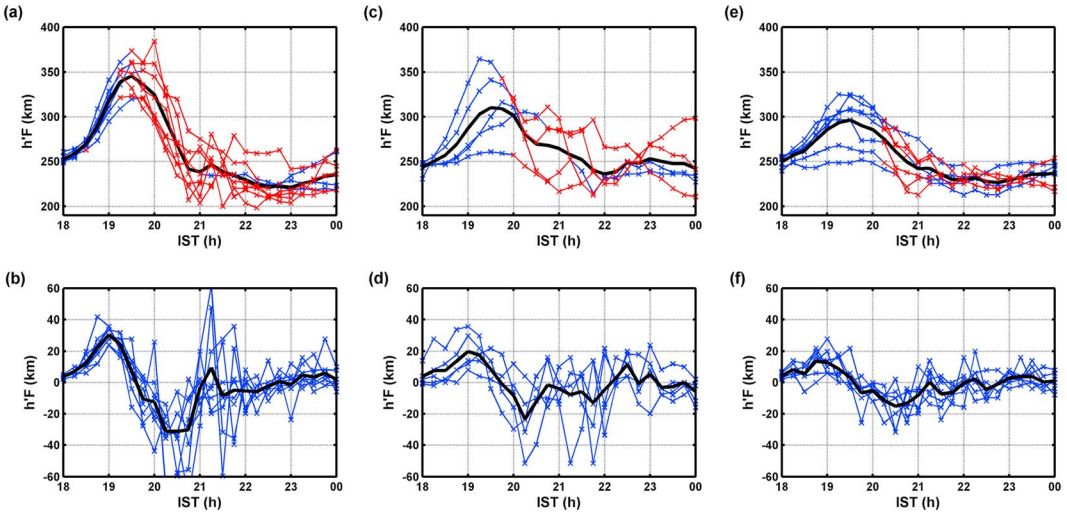

Figure 3. The (a) *h'F* and (b) V_Z, respectively, for early spread *F* onset cases. (c and d) The same as for Figures 3a and 3b but for the moderately delayed spread *F* onset cases. The (e) *h'F* and (f) V_Z, respectively, for the late onset cases. Blue color symbol/line has been used to indicate the presence of classical *F* layer trace, while red color symbol/line indicates spread *F*.

general less than those for the early spread *F* onset cases. Average peak *h'F* and peak V_Z in this case was also less than that corresponding to early spread *F* onset cases.

F layer height migration and the V_Z corresponding to the late spread *F* onset cases (where the onset of spread *F* was delayed by 45 min or more with respect to the time of *F* layer attaining the peak height) are presented in Figures 3e and 3f, respectively. Peak *h'F* for all the cases in this category was less than 350 km. Also, the average value of peak *h'F* was ~300 km. This value is ~50 km less than that for the early spread *F* onset cases. Also, the V_Z was quite less than that in the previous categories. However, on an average, the time of reversal of electric field (zero V_Z) was nearly similar in the three categories. Thus, in the second and third categories, the onset of spread *F* in the ionograms was observed during a time when zonal electric field was westward (V_Z negative). One can note that in a few nights corresponding to the second and third categories, the ESF has occurred despite insignificant height rise of the *F* layer. This is in accordance with the report by *Tsunoda et al.* [2010], of the ESF in the absence of *F* layer height rise but in the presence of LSWS. The peak height attained by the *F* layer and the peak V_Z associated with the prereversal enhancement of zonal field in the early (Category 1) and late (Category 3) spread *F* onset cases are also indicated in Table 1. For the early onset cases the peak V_Z and *h'F* were significantly larger than those for the late onset cases.

Table 1. Peak Vertical Plasma Drift (V_Z) and Peak *h'F* in Early and Late Spread *F* Onset Cases

Date	Peak V_Z (m/s)	Peak *h'F* (km)
	Early Spread F Onset Cases	
24 Feb 2004	25	322
6 Mar 2004	25	325
8 Mar 2004	36	350
19 Mar 2004	30	365
23 Mar 2004	35	360
24 Mar 2004	43	385
25 Mar 2004	35	355
27 Mar 2004	32	355
	Late Spread F Onset Cases	
21 Feb 2004	8	255
5 Mar 2004	13	269
13 Mar 2004	20	298
14 Mar 2004	21	310
20 Mar 2004	22	310
22 Mar 2004	24	328
29 Mar 2004	28	328

In Figure 3, while the mean V_Z in the three categories varied smoothly with time, individual cases show large fluctuations in V_Z. Particularly, the fluctuations in the V_Z occurred after the onset of ESF. It needs mention that after the onset of the ESF, height of the *F* layer in the ionosonde is basically represented by the minimum range of the *F* region irregularity. These irregularities are not spatially homogeneous and also drift eastward. As a result, it produces fluctuations in the *F* layer height measurement, which in turn creates fluctuations in the V_Z measurements.

Table 2. Ionogram Satellite Traces in Early and Late Spread *F* Onset Cases

Date	Satellite Trace Timing (IST)	2F Satellite Trace Timing (IST)
	Early Spread F Onset Cases	
24 Feb 2004	18:45, 19:30	18:45
6 Mar 2004	19:15	Nil
8 Mar 2004	19:00	Nil
19 Mar 2004	Nil	Nil
23 Mar 2004	19:15	Nil
24 Mar 2004	18:45	Nil
25 Mar 2004	19:00, 19:15	19:00
27 Mar 2004	19:30	Nil
	Late Spread F Onset Cases	
21 Feb 2004	Nil	Nil
5 Mar 2004	Nil	Nil
13 Mar 2004	Nil	Nil
14 Mar 2004	19:30, 19:45	Nil
20 Mar 2004	18:45, 19:30	Nil
22 Mar 2004	Nil	Nil
29 Mar 2004	Nil	Nil

3.2.1. Observation of Satellite Traces in the Ionograms

LSWS manifests in different forms in different observational techniques. Satellite traces in the ionograms and their relation to the formation of ESF have been evaluated by *Abdu et al.* [1981]. It has been found that the ESF is often preceded by the observation of satellite traces in the ionograms. Satellite traces appear different from the spread *F*. Often the satellite trace appears just above the 2F trace in the ionogram [*Tsunoda*, 2008], and it has also been regarded as a manifestation of the LSWS. Thus, ionosonde can enable one to observe the precursors of the ESF with ease and without much experimental complexities. Occurrence of satellite traces in the ionograms recorded at Sriharikota has also been analyzed. Table 2 presents the occurrence time of the satellite traces in the early (Category 1) and late (Category 3) spread *F* onset cases. Except on one night, satellite traces were observed prior to the ESF in the first category cases, while the satellite traces were observed only in two nights corresponding to the third category.

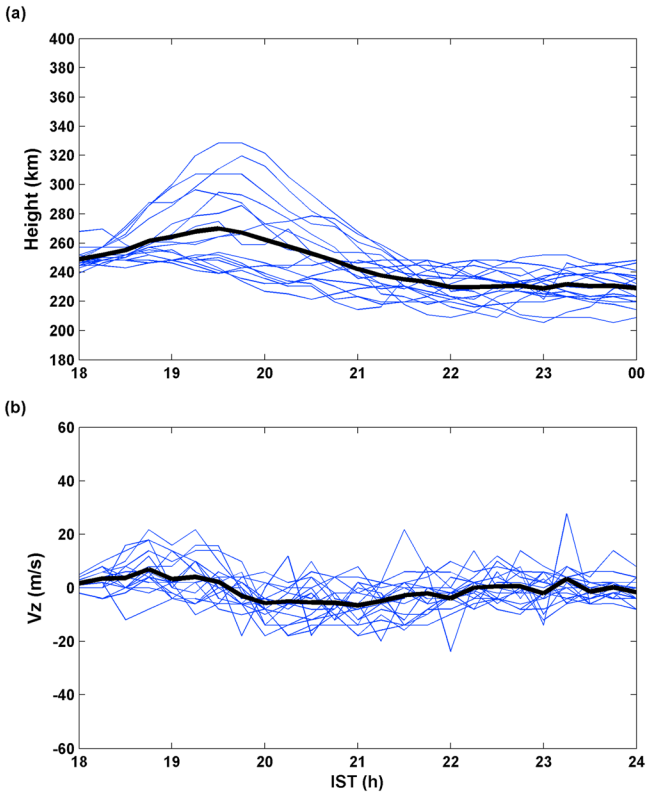

Figure 4. The (a) *h'F* and (b) V_Z on 18 non-spread *F* nights during 15 February to 2 April period.

3.3. *F* Layer Height Migration in Non-ESF Nights

Although, several investigations have highlighted the importance of LSWS in the formation of ESF, some investigations suggest the LSWS to be a necessary, may not be a sufficient condition for the formation of ESF [e.g., *Li et al.*, 2012]. It thus makes sense to also evaluate the height migration of *F* layer in non-ESF nights. Out of 48 nights of observations, ESF did not appear for 18 nights. *F* layer height migration (*h'F*) and the V_Z corresponding to the 18 non-ESF nights are shown in Figures 4a and 4b,

respectively. Although the *F* layer was found to attain the peak height as high as 340 km in some cases, in most nights, the *F* layer height rise was quite insignificant. Also, the V_Z values in the non-ESF nights were, in general, lesser than those for the ESF nights.

4. Discussion

This paper basically relates the onset time of the equatorial spread *F* and the post sunset height rise of the *F* layer. While the *F* layer was found to attain peak height (peak *h'F*) before 19:45 IST in most cases, the onset of spread *F* have not been observed to happen at that time in most cases. *Kelley et al*. [1979] discussed the generalized RT instability, where, in addition to the ion-neutral collision frequency and plasma density gradient, the zonal electric field also influences the growth rate of the RT instability. Eastward electric field acts similar to gravity in destabilizing the plasma; however, its contribution to the linear growth rate of the instability does not vary with the altitude. Thus, the genesis of the EPB is expected to happen either at a time when *F* layer reaches its peak altitude (peak *h'F*) or before that. Late onset of spread *F* most dominantly indicate the genesis of the EPB over a westward longitude, though fresh evolutionary type plasma bubble is also likely to be observed with a delay. Once originated, EPB drift eastward. Onset of spread *F* in the ionosonde depends whether the irregularities are present in the field of view of the ionosonde or not. Irregularities originating at a westward location will manifest as spread *F* at a time when they reach within the field of view of the ionosonde. Assuming the genesis of *F* region irregularities to have occurred at the peak *h'F* time, late onset of spread *F* indicates that the irregularities were not freshly generated. In fact, this is the most likely assumption, as the eastward electric field favors the onset of the RT instability; however, if the onset of the RT instability happens at a time when the zonal field is westward (i.e., after the *F* layer attaining the peak height), even a locally generated EPB will be observed with a delay with respect to the peak *h'F* time. Results presented in this manuscript are, however, discussed assuming that the onset of RT instability happens before peak *h'F* time.

Height migration, as well as vertical plasma drifts of the F layer, has been presented in Figure 3 for the early, moderately delayed, and late spread *F* onset cases. In the early onset cases the peak *h'F* over Sriharikota was, in general, more than that in the moderately delayed and late onset cases. Also, the average peak *h'F* corresponding to the first category was found to be ~35 km higher than that in the second category and ~50 km higher than in the third category. However, the time of *F* layer attaining the peak height was more or less similar in the three categories. The significant difference in the average peak *h'F* in the three categories can lead one to think of a zonal variation of peak *h'F*. This indicates the presence of a large-scale wave structure [*Tsunoda and white*, 1981]. It is quite plausible to think that in the early (moderately delayed and late) onset cases the crest (trough) of the standing large-scale wave structure was located above the ionosonde, i.e., over Sriharikota longitude. Irregularities, however, originated only close to the crest region and drifted eastward. Thus, in the second and third categories, the spread *F* irregularities were observed with a significant delay with respect to the time of *F* layer attaining the peak height. *Tsunoda and Ecklund* [2007] suggested that the extra eastward electric field component (in addition to the eastward electric field associated with the PRE of zonal field) associated with the LSWS can be the missing link in explaining the variability of ESF. Larger values of V_Z observed in the early spread *F* onset cases further corroborate the results of *Tsunoda and Ecklund* [2007]. In addition to it, the large-scale wave can produce a tilt in the ionosphere and can become unstable to wind-driven cross-field instability [*Kelley et al*., 1981; *Tsunoda*, 1983].

Previous investigations have indicated that the LSWS can originate much before the *F* region sunset time [*Thampi et al*., 2009; *Tsunoda et al*., 2011]. Thus, its detection was also made much before the onset of the ESF. Average vertical plasma drift (V_Z) in the early onset cases was slightly greater than that in the late onset cases, in the 18–19 IST periods itself (as shown in Figure 3). Thus, the observations presented in this manuscript are in compliance with those reported earlier. Also, *Tulasi Ram et al*. [2012, 2014a] have shown that the LSWS can be observed spatially a few degrees west of the *E* and *F* region sunset terminators (i.e., before the *E* and *F* region sunset times).

Several investigations have revealed that plasma bubble could also be of evolutionary type appearing around midnight [e.g., *Huang et al*., 2010; *Nishioka et al*., 2012]. However, such observations have been found to occur during the summer months (June, July, and August) of low to moderate solar activity periods. Also, the midnight spread *F* is often preceded by *F* layer height rise. In this manuscript, only the equinox period

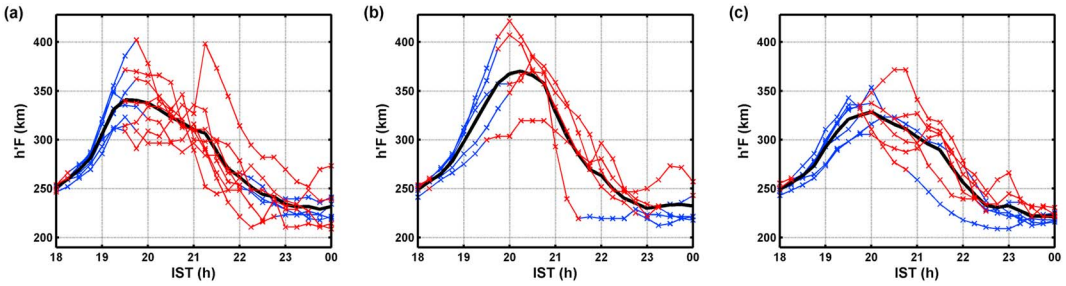

Figure 5. (a–c) The *h'F* recorded by Thumba ionosonde corresponding to the days discussed in Figure 3.

(February, March, and April) observations have been considered. During the equinox period, plasma bubbles are known to be generated at the time of the *F* layer attaining the peak height, when the ionosphere is most unstable under the RT instability. This is based on an assumption that the RT instability maximizes with the intensification of the zonal electric field associated with the prereversal enhancement. However, this assumption is likely to fail if the genesis of the EPB happens after the electric field reversal from eastward to westward. In such a scenario, locally generated fresh EPB will also be observed with a significant delay with respect to the peak *h'F* time. Results presented in this manuscript are indeed consistent with irregularities generated to the west and then drifting into the field of view of the Sriharikota ionosonde, but this cannot be proven for all cases considering the experimental limitations. This assumption can be verified using simultaneous Airglow imager and ionosonde observations as the longitudinal origin of the EPB can be exactly determined using the airglow imager, while ionosonde can be utilized to measure the *F* layer height.

Another important aspect related with the early manifestation of the LSWS is the appearance of the satellite traces in the ionograms. Timings of the appearance of satellite traces in the ionograms, in the two cases, have been indicated in Table 2. One can note that, while satellite trace was not seen only on one night in the first category, it was observed only on two nights corresponding to the third category. Lesser appearance of satellite traces in the third category also gives some indication that the corrugations in the *F* layer responsible for satellite traces were not located overhead (within the field of view of the ionosonde). It gives an impression that in the third category cases it was the trough of the large-scale wave that was located over Sriharikota, while in the first category the soundings were made of a region located in the vicinity of the crest of the large-scale wave.

Observations corresponding to 18 non-ESF nights have also been presented in Figure 4. The *F* layer height rise in non-ESF cases (Figure 4a) has some resemblance with the late spread *F* onset cases (Figure 3e). Five of the non-ESF cases have the peak *h'F* comparable to or larger than the average peak *h'F* of late spread *F* onset cases. This implies that, while the *F* layer height plays the most dominant role in the EPB genesis, it alone does not determine the occurrence of the EPB. Might be, in the five non-ESF cases with significant *F* layer height rise, bottomside sinusoidal zonal plasma density variation capable of seeding the RT instability was absent. Thus, the seeding is likely to be as important a factor as the *F* layer height. Recently, *Li et al.* [2012] have indicated that the seed perturbation alone is not the sufficient criterion for the ESF to occur, as the *F* layer height rise plays a dominant role. Thus, the results presented in this manuscript are in good accordance with *Li et al.* [2012]. Occurrence of the EPB is likely to depend on more than one parameter, including the *F* layer height, seed perturbation, and the LSWS.

4.1. *F* Layer Height Migration Over Thumba

Spatial observation of *F* layer height rise can play an important role in resolving the spatial LSWS features. However, it will be limited by the spatial separation between the observing stations and the scale size of the LSWS. Thumba (8.53°N, 76.87°E) is an equatorial (magnetic equator) station in India and is located ~360 km west of Sriharikota and houses a digital ionosonde. Although there exists a latitudinal difference of ~7° between Sriharikota and Thumba, simultaneous ionosonde observations from these locations can still be used to observe the longitudinal differences in the postsunset height rise of *F* layer. Thus, to study the longitudinal feature of the *F* layer height rise, the height migration of the *F* layer over Thumba (based on Thumba ionosonde observations) has been examined for the cases discussed in Figure 3. Figure 5 shows the

h′F observed over Thumba corresponding to the nights discussed in Figure 3. Figure 5a shows the *h*′*F* over Thumba corresponding to the early onset cases discussed in Figure 3a; *h*′*F* over Thumba corresponding to the moderately delayed spread *F* cases discussed in Figure 3b has been indicated in Figure 5b. The *h*′*F* over Thumba corresponding to the late spread *F* cases discussed in Figure 3c is shown in Figure 5c. Two of the important aspects of the Thumba observations are as follows: (1) spread *F* onset in all the three categories occurred mostly at the time of *F* layer attaining the peak height and (2) the relative magnitude of *F* layer height rise in the three categories differed from that in Figure 3. As far as the onset time of ESF is concerned, ionosonde located at magnetic equator is more likely to observe the bottom type spread F prior to the occurrence of topside spread *F* (which may not be the case with the low-latitude observation). Coming to the *F* layer height rise over Thumba; unlike in Figure 3, where category 1 cases attained the maximum height, in Figure 5, the maximum height was attained by the category 2 cases. The cases belonging to the third category displayed the least average height rise over Thumba, as shown in Figure 5c. Thus, it gives us some indication that in the first category cases, the crest (trough) of the large-scale wave was located in the vicinity of Sriharikota (Thumba) longitude, whereas in the second category cases, the trough (crest) of the large-scale wave was located in the vicinity of Sriharikota (Thumba) longitude, as supported by the fact that average height rise of Category 1 (Category 2) cases was maximum in Figure 3 (Figure 5).

Another important aspect is that the average peak *h*′*F* over Sriharikota, corresponding to the third category (where the onset of the ESF over Sriharikota was delayed by more than 45 min with respect to the peak *h*′*F* time), was ~50 km less than that corresponding to the first category (as can be seen in Figure 3), whereas over Thumba, the average peak *h*′*F* difference between the first and the third categories was just ~10 km (as can be seen in Figure 5). Possibly, in the third category cases, the zonal separation of the crest and the trough of the concerned large-scale wave was significantly larger than the zonal separation between Thumba and Sriharikota (i.e., 360 km). This possibility is further corroborated by the fact that spread *F* onset over Sriharikota in the third category happened after a larger delay with respect to the peak *h*′*F* time than that in the second category. This is just one possibility, which cannot be verified by just two zonally separated ionosondes. Continuous observations using three or more zonally separated ionosondes will be required to derive the exact structure of the LSWS; however, such a network of ionosonde does not exist. Nonetheless, the difference in the Sriharikota and Thumba *h*′*F* observations, corresponding to the three different categories, still indicates that the height rise of the *F* layer was not zonally uniform. This in turn gives some indications of the presence of large-scale wave.

5. Summary and Concluding Remarks

The time of *F* layer attaining the peak height (peak *h*′*F*), the onset time of spread *F* and its relation with the peak *h*′*F* have been investigated using the Sriharikota ionosonde observations of 15 February 2004 to 2 April 2004 (48 days) period. The distribution of peak *h*′*F* time and spread *F* onset time differed significantly, indicating that the time of spread *F* onset in many cases differed from the time of *F* layer attaining the peak height. Average peak *h*′*F* in the early spread *F* onset cases was found to be ~50 km, more than that in the late spread *F* onset cases. This can be explained if a standing large-scale wave structure is assumed to exist in the bottomside of *F* layer. However, the exact magnitude of the large-scale wave on a particular evening can only be inferred using the zonal measurement of *F* layer height. Other popular techniques like satellite traces, multireflected echo traces, scanning airglow photometers, and total electron content measurements using C/NOFS (Communication and Navigation Outages forecasting system) can also be used to monitor the presence of large-scale waves. However, these techniques provide an integrated picture and scarcely reveal the precise structure of the large-scale waves in terms of its amplitude and *F* layer height. Thus, the continuous zonal measurement of *F* layer height will be required to infer the exact structure of the large-scale wave (amplitude, phase, and height) and its impact on the stability of the evening *F* layer.

Acknowledgments

The author is thankful to Indian Institute of Geomagnetism for providing Nanabhoy Moos postdoctoral fellowship. The author is also grateful to A.K. Patra for providing the Sriharikota ionosonde data. Sriharikota and Thumba ionosonde data can be obtained by contacting A.K. Patra (akpatra@narl.gov.in) and T.K. Pant (tarun_kumar@vssc.gov.in), respectively.

References

Abdu, M. A., I. S. Batista, and J. A. Bittencourt (1981), Some characteristics of spread *F* at the magnetic equatorial station Fortaleza, *J. Geophys. Res.*, *86*(A8), 6836–6842, doi:10.1029/JA086iA08p06836.

Abdu, M. A., R. T. deMedeiros, J. A. Bittencourt, and I. S. Batista (1983), Vertical ionization drift velocities and range type spread *F* in the evening equatorial ionosphere, *J. Geophys. Res.*, *88*(A1), 399–402, doi:10.1029/JA088iA01p00399.

Aquino, M., and V. Sreeja (2013), Correlation of scintillation occurrence with interplanetary magnetic field reversals and impact on Global Navigation Satellite System receiver tracking performance, *Space Weather*, *11*, 219–224, doi:10.1002/swe.20047.

Bagiya, M. S., R. Sridharan, and S. Sunda (2013), Pre-assessment of the "strength" and "latitudinal extent" of L-band scintillation: A case study, *J. Geophys. Res. Space Physics*, *118*, 488–495, doi:10.1029/2012JA017989.

de Lima, G. R. T., S. Stephany, E. R. de Paula, I. S. Batista, M. A. Abdu, L. F. C. Rezende, M. G. S. Aquino, and A. P. S. Dutra (2014), Correlation analysis between the occurrence of ionospheric scintillation at the magnetic equator and at the southern peak of the equatorial ionization anomaly, *Space Weather*, *12*, 406–416, doi:10.1002/2014SW001041.

Farley, D. T., E. Bonelli, B. G. Fejer, and M. F. Larsen (1986), The prereversal enhancement of the zonal electric field in the equatorial ionosphere, *J. Geophys. Res.*, *91*(A12), 13,723–13,728, doi:10.1029/JA091iA12p13723.

Haerendel, G., and J. V. Eccles (1992), The role of the equatorial electrojet in the evening ionosphere, *J. Geophys. Res.*, *97*(A2), 1181–1192, doi:10.1029/91JA02227.

Huang, C.-S., O. de La Beaujardiere, R. F. Pfaff, J. M. Retterer, P. A. Roddy, D. E. Hunton, Y.-J. Su, S.-Y. Su, and F. J. Rich (2010), Zonal drift of plasma particles inside equatorial plasma bubbles and its relation to the zonal drift of the bubble structure, *J. Geophys. Res.*, *115*, A07316, doi:10.1029/2010JA015324.

Huang, C.-S., O. de La Beaujardière, P. A. Roddy, D. E. Hunton, J. O. Ballenthin, M. R. Hairston, and R. F. Pfaff (2013), Large-scale quasiperiodic plasma bubbles: C/NOFS observations and causal mechanism, *J. Geophys. Res. Space Physics*, *118*, 3602–3612, doi:10.1002/jgra.50338.

Kelley, M. C., K. D. Baker, and J. C. Ulwick (1979), Late time barium cloud striations and their possible relationship to equatorial spread *F*, *J. Geophys. Res.*, *84*(A5), 1898–1904, doi:10.1029/JA084iA05p01898.

Kelley, M. C., M. F. Larsen, C. LaHoz, and J. P. McClure (1981), Gravity wave initiation of equatorial spread *F*: A case study, *J. Geophys. Res.*, *86*(A11), 9087–9100, doi:10.1029/JA086iA11p09087.

Kelly, M. A., J. M. Comberiate, E. S. Miller, and L. J. Paxton (2014), Progress toward forecasting of space weather effects on UHF SATCOM after Operation Anaconda, *Space Weather*, *12*, 601–611, doi:10.1002/2014SW001081.

Li, G., B. Ning, M. A. Abdu, W. Wan, and L. Hu (2012), Precursor signatures and evolution of post-sunset equatorial spread-*F* observed over Sanya, *J. Geophys. Res.*, *117*, A08321, doi:10.1029/2012JA017820.

Nishioka, M., Y. Otsuka, K. Shiokawa, T. Tsugawa, Effendy, P. Supnithi, T. Nagatsuma, and K. T. Murata (2012), On post-midnight field-aligned irregularities observed with a 30.8-MHz radar at a low latitude: Comparison with *F*-layer altitude near the geomagnetic equator, *J. Geophys. Res.*, *117*, A08337, doi:10.1029/2012JA017692.

Oladipo, O. A., J. O. Adeniyi, A. O. Olawepo, and P. H. Doherty (2014), Large-scale ionospheric irregularities occurrence at Ilorin, Nigeria, *Space Weather*, *12*, 300–305, doi:10.1002/2013SW000991.

Patra, A. K., A. Taori, P. P. Chaitanya, and S. Sripathi (2013), Direct detection of wavelike spatial structure at the bottom of the *F* region and its role on the formation of equatorial plasma bubble, *J. Geophys. Res. Space Physics*, *118*, 1196–1202, doi:10.1002/jgra.50148.

Sastri, J. H., M. A. Abdu, I. S. Batista, and J. H. A. Sobral (1997), Onset conditions of equatorial (range) spread *F* at Fortaleza, Brazil, during the June solstice, *J. Geophys. Res.*, *102*(A11), 24,013–24,021, doi:10.1029/97JA02166.

Shume, E. B., A. J. Mannucci, M. D. Butala, X. Pi, and C. E. Valladares (2013), Flux tube analysis of L-band ionospheric scintillation, *J. Geophys. Res. Space Physics*, *118*, 3791–3804, doi:10.1002/jgra.50285.

Sreeja, V., M. Aquino, and Z. G. Elmas (2011), Impact of ionospheric scintillation on GNSS receiver tracking performance over Latin America: Introducing the concept of tracking jitter variance maps, *Space Weather*, *9*, S10002, doi:10.1029/2011SW000707.

Sreeja, V., M. Aquino, Z. G. Elmas, and B. Forte (2012), Correlation analysis between ionospheric scintillation levels and receiver tracking performance, *Space Weather*, *10*, S06005, doi:10.1029/2012SW000769.

Thampi, S. V., M. Yamamoto, R. T. Tsunoda, Y. Otsuka, T. Tsugawa, J. Uemoto, and M. Ishii (2009), First observations of large-scale wave structure and equatorial spread *F* using CERTO radio beacon on the C/NOFS satellite, *Geophys. Res. Lett.*, *36*, L18111, doi:10.1029/2009GL039887.

Tsunoda, R. T. (1983), On the generation and growth of equatorial backscatter plumes: 2. Structuring of the west walls of upwellings, *J. Geophys. Res.*, *88*(A6), 4869–4874, doi:10.1029/JA088iA06p04869.

Tsunoda, R. T. (2008), Satellite traces: An ionogram signature for large-scale wave structure and a precursor for equatorial spread *F*, *Geophys. Res. Lett.*, *35*, L20110, doi:10.1029/2008GL035706.

Tsunoda, R. T. (2009), Multi-reflected echoes: Another ionogram signature of large-scale wave structure, *Geophys. Res. Lett.*, *36*, L01102, doi:10.1029/2008GL036221.

Tsunoda, R. T., and W. L. Ecklund (2007), On the post-sunset rise of the equatorial *F* layer and superposed upwellings and bubbles, *Geophys. Res. Lett.*, *34*, L04101, doi:10.1029/2006GL028832.

Tsunoda, R. T., and B. R. White (1981), On the generation and growth of equatorial backscatter plumes: 1. Wave structure in the bottomside *F* layer, *J. Geophys. Res.*, *86*(A5), 3610–3616, doi:10.1029/JA086iA05p03610.

Tsunoda, R. T., D. M. Bubenik, S. V. Thampi, and M. Yamamoto (2010), On large-scale wave structure and equatorial spread *F* without a post-sunset rise of the *F* layer, *Geophys. Res. Lett.*, *37*, L07105, doi:10.1029/2009GL042357.

Tsunoda, R. T., M. Yamamoto, T. Tsugawa, T. L. Hoang, S. Tulasi Ram, S. V. Thampi, H. D. Chau, and T. Nagatsuma (2011), On seeding, large-scale wave structure, equatorial spread *F*, and scintillations over Vietnam, *Geophys. Res. Lett.*, *38*, L20102, doi:10.1029/2011GL049173.

Tulasi Ram, S., P. V. S. Rama Rao, D. S. V. V. D. Prasad, K. Niranjan, S. Gopi Krishna, R. Sridharan, and S. Ravindran (2008), Local time dependant response of post-sunset ESF during geomagnetic storms, *J. Geophys. Res.*, *113*, A07310, doi:10.1029/2007JA012922.

Tulasi Ram, S., M. Yamamoto, R. T. Tsunoda, S. V. Thampi, and S. Gurubaran (2012), On the application of differential phase measurements to study the zonal large scale wave structure (LSWS) in the ionospheric electron content, *Radio Sci.*, *47*, RS2001, doi:10.1029/2011RS004870.

Tulasi Ram, S., M. Yamamoto, R. T. Tsunoda, H. D. Chau, T. L. Hoang, B. Damtie, M. Wassaie, C. Y. Yatini, T. Manik, and T. Tsugawa (2014a), Characteristics of large-scale wave structure observed from African and Southeast Asian longitudinal sectors, *J. Geophys. Res. Space Physics*, *119*, 2288–2297, doi:10.1002/2013JA019712.

Tulasi Ram, S., S. Kumar, S.-Y. Su, B. Veenadhari, and S. Ravindran (2014b), The influence of Corotating Interaction Region (CIR) driven geomagnetic storms on the development of equatorial plasma bubbles (EPBs) over wide range of longitudes, *Adv. Space Res.*, *55*, 535–544, doi:10.1016/j.asr.2014.10.013.

Whalen, J. A. (2007), Weather of the postsunset equatorial anomaly recorded daily during 2 years near solar maximum, *Space Weather*, *5*, S01002, doi:10.1029/2006SW000235.

Zhang, D. H., Z. Xiao, M. Feng, Y. Q. Hao, L. Q. Shi, G. L. Yang, and Y. C. Suo (2010), Temporal dependence of GPS cycle slip related to ionospheric irregularities over China low-latitude region, *Space Weather*, *8*, S04D08, doi:10.1029/2008SW000438.

AGU PUBLICATIONS

JGR

Journal of Geophysical Research: Space Physics

RESEARCH ARTICLE
10.1002/2014JA020584

Key Points:
- Unusual depletion of thermospheric dayglow associated with PPEF
- Simultaneous mesopause heating evidenced by ground/space based measurements
- The proposed mechanism vindicated using the magnetometer observations

Correspondence to:
T. K. Pant,
tarun_kumar@vssc.gov.in

Citation:
Sumod, S. G., T. K. Pant, C. Vineeth, and M. M. Hossain (2015), Unusual depletion of OI 630.0 nm dayglow and simultaneous mesopause heating during the penetration of interplanetary electric field over dip equator, *J. Geophys. Res. Space Physics*, *120*, doi:10.1002/2014JA020584.

Received 8 SEP 2014
Accepted 11 JAN 2015
Accepted article online 16 JAN 2015

Unusual depletion of OI 630.0 nm dayglow and simultaneous mesopause heating during the penetration of interplanetary electric field over dip equator

S. G. Sumod[1,2], T. K. Pant[1], C. Vineeth[1], and M. M. Hossain[1]

[1]Space Physics Laboratory, Vikram Sarabhai Space Centre, Trivandrum, India, [2]Department of Physics, S. H. College, Kochi, India

Abstract Evidence for simultaneous changes in the thermosphere and mesopause associated with penetration electric fields using the OI 630.0 nm and OH (8, 3) dayglow measurements are presented. An unusual decrease in the thermospheric OI 630.0 nm dayglow and an intense heating (~30 K) at OH emission altitudes over a magnetic dip equatorial station, Trivandrum, India, were observed on 9 April 2006, coincident with the penetration of a noontime westward interplanetary electric field. The Sounding of the Atmosphere using Broadband Emission Radiometry observations on board TIMED satellite also revealed heating at the mesopause heights during this period. In addition, ionosonde and magnetometer observations indicated the presence of strong penetration electric fields. We propose that strong heating at the mesopause resulted in the intrusion of additional neutrals, like N_2, into the emission altitudes and quenched the O(^{1}D) atoms therein. The reduced Cowling conductivity at the *E* region inferred using magnetometer observations further corroborates this proposed mechanism.

1. Introduction

The prompt penetration electric fields (PPEFs) and their effects in the ionospheric region over the equatorial and low latitudes have generated great scientific interest in recent years [*Kikuchi et al*., 2010; *Sreeja et al*., 2011, and references therein]. These fields basically arise from either the prevailing undershielding/overshielding conditions in the magnetosphere [e.g., *Fejer et al*., 2007] or due to the divergence of asymmetric ring currents and increased polar cap potential drop [e.g., *Senior and Blanc*, 1984]. The undershielding/overshielding fields are eastward/westward during day and westward/eastward during nighttime, corresponding to the southward/northward turning of interplanetary magnetic field (IMF) B_z. The temporal, longitudinal, and latitudinal variations of the effect of PPEFs have been addressed in recent years from both experimental and theoretical perspectives [*Fejer et al*., 1990]. Studies have also been carried out to understand the efficiency, i.e., the ratio of the change in equatorial ionospheric electric field to that of the interplanetary electric field [e.g., *Manoj et al*., 2008] and the characteristic time scale of penetration, i.e., the time within which the interplanetary electric field penetrates to the low-latitude ionosphere without shielding [e.g., *Huang et al*., 2005].

The effects of penetration events over the dynamo region were first reported using magnetometer observations [*Nishida*, 1968]. Several studies since then have shown the impact of PPEFs over the *F* region using coherent/incoherent scatter radars [*Huang et al*., 2005] and ionosonde observations [*Balan et al*., 2008]. Simultaneous effects of PPEFs over *E* and *F* regions of equatorial ionosphere have also been studied [*Sreeja et al*., 2011].

Although there is mounting evidence showing the signatures of PPEFs in the dynamo and *F* region over the equator/low-latitude ionosphere, there had been no observations indicating, directly or indirectly, the effect of PPEFs in the mesopause region. In this context, this study presents observations made on 9 April 2006, which are indicative of the manifestation of PPEFs, not only in the equatorial ionosphere-thermosphere system but also in the mesopause region. The study shows the evidence for strong neutral heating in the equatorial mesopause region and unusual quenching in daytime OI 630.0 airglow emissions associated with the penetration events, probably for the first time.

2. Experiment

The intensity of OI 630.0 nm dayglow emissions from the thermosphere and hydroxyl OH (8, 3) emissions at wavelengths 731.6 and 740.2 nm from the mesopause altitudes were measured using the unique Multiwavelength Dayglow Photometer (MWDPM), over the dip equatorial station Trivandrum (8.5°N, 77°E, dip 0.5°N), India. These dayglow measurements using MWDPM had been extensively used to investigate various aspects of the coupling processes in the equatorial mesosphere-lower thermosphere-ionosphere (MLTI) region [e.g., *Pant et al*., 2007; *Vineeth et al*., 2007; *Sumod et al*., 2014]. The comprehensive details of this system and data analysis procedure have been published elsewhere [*Sridharan et al*., 1998]. The system scanned the sky at five different elevations south of Trivandrum, the minimum elevation being 66° and maximum 90°. In this configuration, the farthest points of observation for thermosphere and mesopause are ~550/225 km from zenith, considering the OI 630.0 and OH emission peak at ~220 and 90 km, respectively. The dayglow measurements on 9 April 2006 were made at high cadence (~7.5 min) between 08:00 IST (Indian standard time =UT + 5.5 h) and 18:00 IST at different elevations as mentioned above.

The mesopause temperature (MT) was derived using the OH emissions over Trivandrum obtained from MWDPM, following the intensity ratio method as described by *Meriwether* [1975]. In the present case, the relative intensities of the two rotational lines 731.6 and 740.2 nm of the same vibrational band (P_1 (5) and P_1 (2)) have been used. These vibrationally excited OH molecules are in local thermodynamic equilibrium due to their sufficiently long lifetime in the excited state as compared to the intercollisional period [*Krassovsky*, 1972]. Therefore, the calculated rotational temperatures are considered as a good measure of the ambient temperature. Under the assumption that the population of the excited state follows Maxwell-Boltzmann distribution, the quantum mechanical calculations yield the temperature in terms of the ratio of the intensities of these two rotational lines. The maximum error associated with the MT measurements is found to be less than ±7 K [*Sridharan et al*., 1999]. Further, temperature profiles estimated using CO_2 emissions at 15 μm measured through Sounding of the Atmosphere using Broadband Emission Radiometry (SABER) on board TIMED satellite were also analyzed.

Simultaneous high-cadence (~5 min) measurements of the critical frequency (f_oF_2) and peak height (h_mF_2) of the ionospheric F_2 region were obtained using a collocated KEL digital ionosonde. The strength of the surface magnetic field measured every minute over Trivandrum (ΔH_{TVM}), an equatorial electrojet (EEJ) station, and Alibag (ΔH_{ABG}) (18.6°N, 72.9°E, dip 12.8°N), an off-EEJ station, has been used to obtain the variability associated with the EEJ. These magnetic field measurements essentially represent the equatorial zonal electric field and conductivity changes in the dynamo region. The symbols $\Delta H_{TVM/ABG}$ stand for the difference in the instantaneous values of horizontal component of magnetic field from its nighttime mean value for Trivandrum and Alibag, respectively.

In order to assess the prevailing geomagnetic conditions on 9 April 2006 ($Ap = 46$), the high-resolution (~5 min) data of interplanetary magnetic field (IMF B_z) and dawn-dusk component of interplanetary electric field (IEF E_y) are used. These data were obtained using the OMNI data resource (http://omniweb.gsfc.nasa.gov/). The data have already been time shifted to account for the propagation delay of solar wind transiting from the location of the satellite situated at L_1 point (~1.41×10^6 km from Earth) to the Earth's bow shock nosecone.

3. Geomagnetic Conditions

The month of April 2006 was characterized by moderate solar activity (mean of 10.7 cm solar radio flux index, $F_{10.7}$ being 89), where three major geomagnetic storms took place consecutively during 4–20 April 2006. The second storm started on 9 April 2006 and was relatively intense but of short duration. The ring current on this day reached a maximum (the *SYM-H* index was −108 nT) at ~12:30 IST and recovered thereafter (not illustrated here). The penetration events discussed in this paper happened on 9 April 2006 on the dayside dip equator over the Indian longitudes. For the clear identification of the penetration events, the IMF B_z and dawn-dusk component of IEF E_y are plotted along with equatorial ionospheric parameters in Figure 1. As is evident from Figure 1c, the IMF B_z was oscillating south and northward during the day. Each southward/northward excursion of IMF corresponds to an enhancement of IEF E_y in the duskward/dawnward direction. An additional time lag of ~20 min is introduced in the IEF E_y and IMF B_z in order to correlate

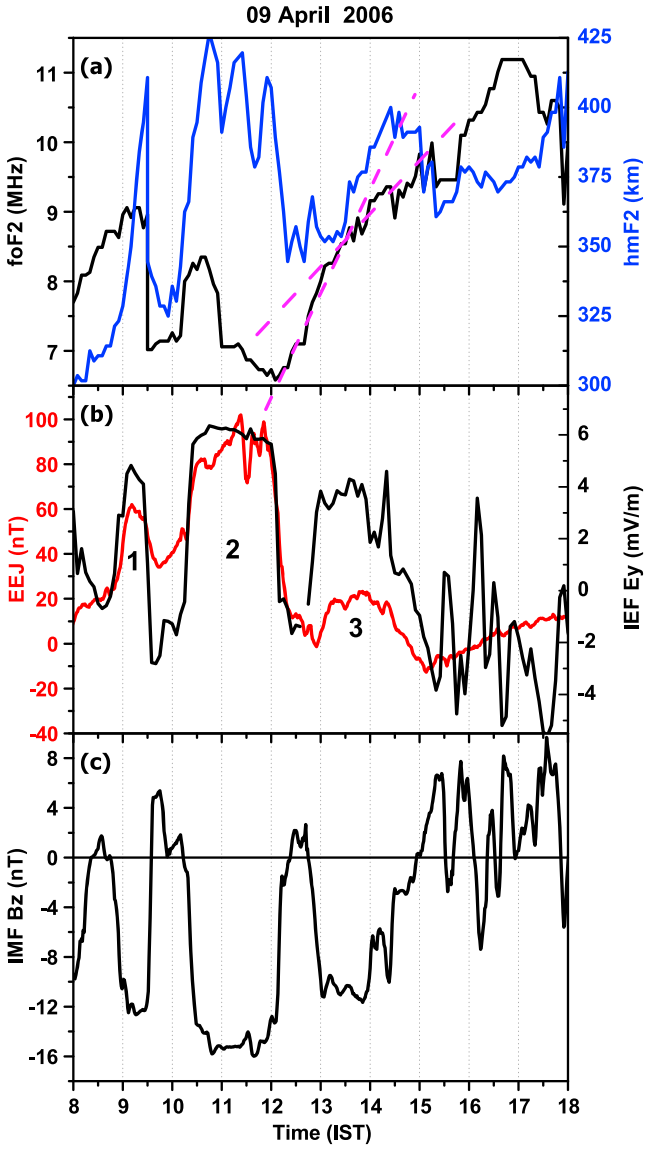

Figure 1. Temporal variation of the equatorial ionospheric parameters (a) f_oF_2 (MHz) and h_mF_2 (km) (b) EEJ (nT) along with the dawn-dusk component of interplanetary electric field (IEF) E_y (mV/m) and (c) IMF B_z (nT) during the penetration events of 9 April 2006.

with equatorial ionospheric observations. This may account for the retardation of solar wind by the bow shock and subsequent acceleration in the magnetosheath. The concomitant variation of the eastward and westward fluctuations in the interplanetary and equatorial zonal electric field during the period of 08:30–15:30 IST vindicates the presence of prompt penetration.

4. Results and Discussion

4.1. Response of Ionosphere/ Thermosphere to the Penetration Event of 9 April 2006.

Figure 1a shows the time variation of f_oF_2 and h_mF_2 on 9 April 2006. For comparison, the mean temporal behavior of f_oF_2 and h_mF_2, which is the quiet time average for three international magnetically quiet days of the month (i.e., 2, 6, and 30 April 2006), is shown in Figure 2 along with their standard deviations. As is evident from the figures, on the event day, both f_oF_2 and h_mF_2 showed a distinctly different pattern in comparison with the normal behavior.

For convenience of description, the three prominent positive pulses in IEF E_y and EEJ are marked as 1, 2, and 3 in Figure 1b. During the rising edge of the first pulse (~08:45 IST), an increase in h_mF_2 (Figure 1a) was observed until ~09:30 IST, which is indicative of an eastward PPEF. The penetrating field increased the f_oF_2 and h_mF_2 during this period through the upward $E \times B$ drift as is evident from Figure 1a. The ascend of the F_2 layer to higher altitudes (~425 km) during this period produced an F_3 layer (not shown here). This resulted in the reduction of f_oF_2 and h_mF_2 until 10:15 IST. The development of F_3 layer due to the PPEF vindicates the mechanism of the formation of F_3 layer due to the combined action of equatorward wind and electric field due to penetration [*Balan et al.*, 2008]. These observations are consistent with many of the earlier studies dealing with the formation of F_3 layers associated with the PPEF from different longitudinal sectors [*Sreeja et al.*, 2011; *Balan et al.*, 2008, and references therein]. As the observations of F_3 layer associated with PPEF have been shown by many of the previous researchers, the description of F_3 layer is not included in the present work.

At ~10:15 IST (the rising edge of the second pulse), the h_mF_2 increased up to 425 km and remained high until ~12:00 IST, indicating a possible eastward penetration. The oscillations seen in h_mF_2 during this period are evident in the EEJ too. However, the PPEF initially increased the f_oF_2 due to the upward $E \times B$ drift until 10:30 IST, thereafter f_oF_2 showed a decrease, which continued until 12:00 IST. This is due to the enhanced

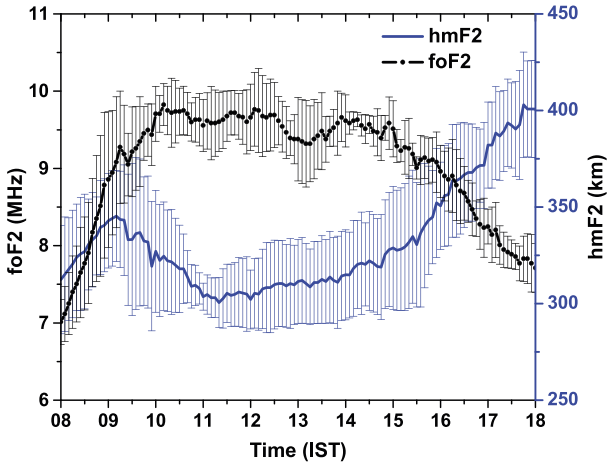

Figure 2. Temporal evolution in the average quiet time variation of f_oF_2 (MHz) and h_mF_2 (km) for the month of April 2006.

plasma diffusion along the field lines to off-equatorial latitudes owing to the fountain effect generated by the prevailing PPEF.

In the falling edge of the second pulse (~12:00 IST), the h_mF_2 showed a decrease which ensued until 12:30 IST, indicating that the penetration occurred in westward phase. This noontime westward penetration resulted in the reverse fountain over equator and an increase in f_oF_2 through the reduced upward $E \times B$ drift. Interestingly, with the westward overshielding electric field at ~12:00 IST, an unusual depletion of the OI 630.0 nm dayglow was observed as is shown in Figure 3. In fact, this depletion was noticed at all elevations and continued for the rest of the day. It is quite unexpected because over the equator, the temporal evolution of the OI 630.0 nm dayglow follows solar zenith angle superposed with electrodynamical variabilities at the emission altitudes (~150–300 km) [*Sumod et al.*, 2012]. The plausible mechanism for the present observations is discussed in the section 4.2.

During the third pulse (13:00–15:00 IST), the eastward PPEF was experienced over equator as evidenced by the concomitant enhancement in h_mF_2 and EEJ during this period. Although the enhanced plasma diffusion to off-equatorial latitudes during this penetration did not decrease the f_oF_2, it reduced the rate of increase of f_oF_2. This is obvious from the difference in the rate of change (slope) of f_oF_2 before and after 13:00 IST, as is indicated using dotted magenta lines in Figure 1a. A further decrease in the h_mF_2 during 15:00–15:30 IST indicates the presence of a westward penetration, as the IMF B_z shows a northward turning during this period. Following this, the equatorial ionosphere behaved more or less similar to the quiet time average, albeit with a few additional fluctuations, which could be attributed to the ensuing storm activities.

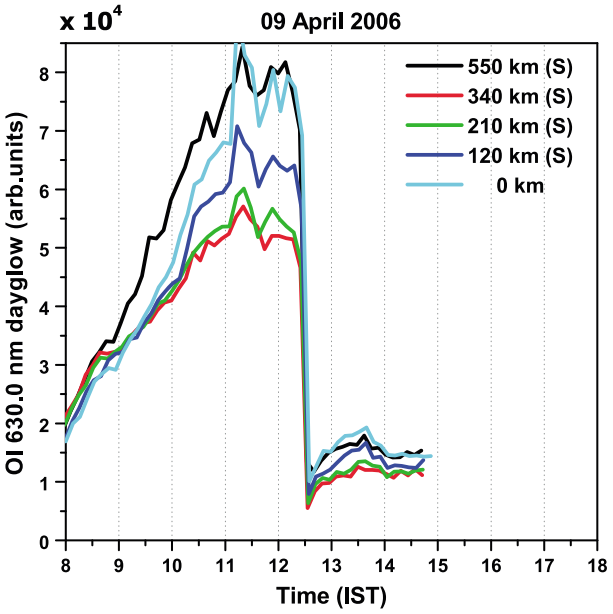

Figure 3. Time evolution of equatorial OI 630.0 nm dayglow on 9 April 2006. The different colors represent the different horizontal distances in kilometers from zenith sky (0 km) over Trivandrum in southern (S) direction.

4.2. Plausible Mechanism for the Unusual Response of OI 630.0 nm Dayglow

As is known, the OI 630.0 nm dayglow is produced due to (i) photoelectron impact of O, (ii) photodissociation of O_2, and (iii) dissociative recombination of O_2^+ ions [*Solomon and Abreu*, 1989]. It is understood that the first two processes follow the solar zenith angle, and the temporal variability seen in the 630 nm dayglow is mainly due to the third process which is closely correlated with the electron density at the emission peak (~220 km) [*Sridharan et al.*, 1992] over low latitudes. The first two processes are not expected to vary abruptly. Further, our

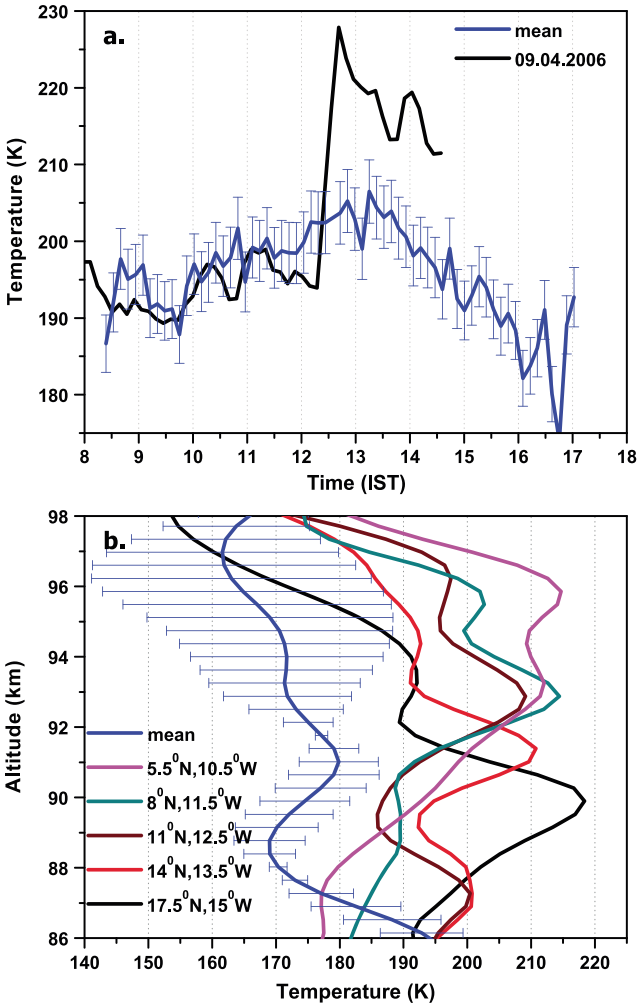

Figure 4. (a) The temporal variation of optically estimated mesopause temperature (MT) on the event day and the monthly mean temperatures during April 2006 along with their standard deviations. (b) The SABER-measured temperature profiles during the event over low latitudes (5°–20°N) for the longitudes (10°–17°W) along with the average of the same on the quiet day with their standard deviations.

observations during the westward electric field at ~12:00 IST showed a clear-cut decrease in h_mF_2 and an increase in f_oF_2. This actually should have increased the dayglow intensity through the increase in dissociative recombination. Therefore, in the present case, the possibility of the reduction in dayglow due to the electrodynamical effects can be excluded. Another possibility of the reduction in airglow intensity can be due to the change in the centroid of the emission. However, the statistical analysis of Wind Imaging Interferometer-measured O(^{1}D) profiles revealed that the emission peak cannot go beyond 220 ± 20 km [*Zhang and Shepherd*, 2004]. Further, we cannot comment on the emission altitude of the OI dayglow emission in the absence of O(^{1}D) profiles over Trivandrum during this time. The third and possibly most important cause of the depletion in OI 630.0 nm dayglow could be due to the quenching of O(^{1}D) atoms because of the intrusion of additional molecular species like N_2 into the emission altitudes. However, the possibility of such a scenario will necessitate a strong heating at the thermospheric altitudes and below (for instance mesopause). In fact, many of the earlier studies have revealed prompt [*Gupta et al.*, 1986] and delayed [*Richmond et al.*, 2003] heating at thermospheric altitudes during geomagnetic storms over equatorial/low latitudes.

In this context, in order to investigate whether there is any increase in the temperature at mesopause altitudes, the temporal evolution of the optically estimated MT using MWDPM on 9 April 2006 is plotted in Figure 4a. For comparison, the mean MTs during the geomagnetic quiet days of April 2006 ($Ap < 7$, Ap being the index representing the planetary level of geomagnetic disturbance) along with their standard deviations are also shown (blue solid lines). As is obvious from the figure, the mesopause exhibited significant heating (~30 K) after 12:15 IST, when the overshielding occurred. The temperature was indeed as high as ~230 K, whereas on normal days, it ranges between 180 and 210 K. The enhancement in MT as seen in the present case is conspicuous, as the dynamical forcing due to waves (gravity/planetary), tides, and chemistry can induce only a temperature difference of about 5–10 K [*Sumod et al.*, 2011a]. Nevertheless, strong changes on the order of ~30 K were also observed using ground based and satellite measurements, for special events like the solar eclipse [*Sumod et al.*, 2011b].

In order to further verify the aforementioned mesopause heating, the SABER observations on board NASA's TIMED satellite have also been looked into. As there were no satellite passes available over equatorial latitudes at Indian longitudes during the penetration event, the temperature profiles over equatorial/low latitudes (5°–20°N) at a different longitude sector (10°–17°W) are considered. These

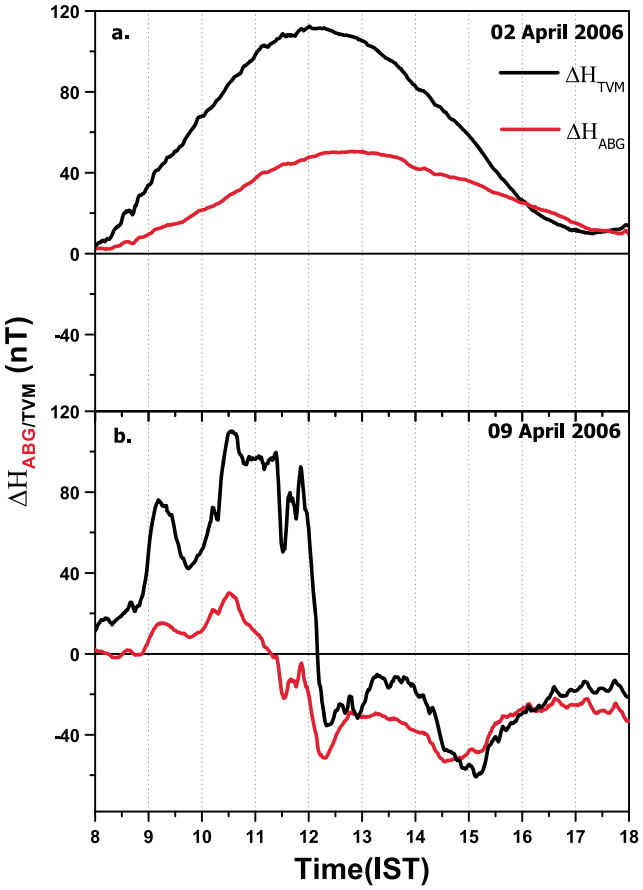

Figure 5. The time variation of ΔH_{TVM} and ΔH_{ABG} separately for (a) a typical geomagnetic quiet day, 2 April 2006 and (b) the event day, 9 April 2006.

passes were at ~06:45 UT, which was 15 min after the penetration event. Figure 4b depicts these temperature profiles on 9 April 2006. The coordinates corresponding to the satellite observations are labeled on the bottom left corner of the figure. The same on the quiet day (2 April 2006) are averaged and plotted (blue line) along with their standard deviations. On this day, the satellite passes were at ~08:00 UT, which is 01:15 h ahead as compared with the event day. This local time difference can produce a maximum change of only ~5–7 ± 2.4 K [*Xu et al.*, 2007]. The enhancement in temperature from SABER measurements is indeed as high as ~30 K for all the profiles on the event day throughout the altitudes ~87–97 km. This strongly corroborates the heating at mesopause as observed by the ground-based MWDPM irrespective of the techniques used for the temperature estimation. Thus, the heating observed at mesopause altitudes provides strong evidence for the unusual quenching of $O(^1D)$ atoms at the emission altitudes through the intrusion of additional molecular N_2.

However, the presence of additional neutrals over the equator due to the heating of the mesopause will decrease the conductivity of the *E* region through increasing the ion-neutral collisions. In fact, earlier studies have revealed a clear-cut connection between the phase velocity changes in the *E* region through ion-neutral collisions and energetics at mesopause altitudes through the changes in composition [*Pant et al.*, 2007]. In this context, the magnetic field measurements at an EEJ station, Trivandrum (ΔH_{TVM}), and a station just outside the EEJ belt, Alibag (ΔH_{ABG}), can better yield this information. The rationale is that during penetration time, the variation which can arise in the current ($J = \sigma E_x$)-induced magnetic field measurements is solely due to the changes in conductivity (σ). It is because the zonal electric field (E_x) is global in nature and should be the same over Trivandrum and Alibag due to the overshielding/undershielding effects in the present case. In fact, the conductivity changes at middle/high-latitude MLTI region associated with the geomagnetic activity are well explored in literature [e.g., *Goldberg et al.*, 1994, and references therein].

Therefore, to understand the changes in conductivity during the overshielding at ~12:00 IST on 9 April 2006, we have analyzed the time evolution of ΔH_{TVM} and ΔH_{ABG} separately and is plotted (Figure 5b) along with the same on a geomagnetically quiet day (Figure 5a). The adjacent days are magnetically disturbed; hence, 2 April 2006 is considered as the quiet day. As is evident from the figure, on the quiet day, a discrete difference in the ΔH values between Trivandrum and Alibag can be noticed throughout the day, which maximizes (~60 nT) at ~12:00 IST. This is due to the enhanced cowling conductivity over the equator during noontime. Nonetheless, this is not the case on 9 April 2006, where the difference in the ΔH_{TVM} and ΔH_{ABG} exists only until 12:00 IST, thereafter it decreases. In fact, the difference was found to be the minimum around noontime,

contrary to that on a quiet day, where it shows a maximum. This indicates that the Cowling conductivity on this day at EEJ altitudes over Trivandrum drastically reduced at ~12:00 IST and thereafter. Thus, the magnetometer observations strongly substantiate the idea that the intense heating at mesopause resulted in drastic decrease in conductivity at dynamo region. This in turn provides strong evidence for the unusual quenching of OI dayglow observed during the westward penetration time due to the intrusion of additional molecular species like N_2 into the emission altitudes.

The simultaneity of the change in IMF B_z and heating at mesopause vindicates that the observed effects are due to the overshielding. It is well known that during the overshielding, the enhanced convection electric field drives an earthward motion of plasma in the plasmasheet, generating a partial ring current and the Region 2 field-aligned currents (R2 FACs) in the inner magnetosphere. This R2 FACs generate an electric field in the ionosphere with an opposite direction to that of the convection electric field at middle and low latitudes. Therefore, over the dip equator, a reduction in the zonal electric field and hence the counter electrojet (CEJ) is anticipated. Further, it should be noted that the equatorial CEJ is connected with the R2 FACs via the auroral ionosphere [*Kikuchi et al*., 2011; *Simi et al*., 2012]. Thus, the overshielding field would produce an increased westward current. In the present case, it has been observed that this current increased the ion-neutral collisions over the equator and reduced the equatorial Cowling conductivity, as discussed above. This in turn resulted in an increase in mesopause temperature. As the CEJ and the mesopause energetics are highly modulated by common forcings such as tides or the gravity/planetary waves, the plausibility of their roles cannot be precluded in this context. However, in the absence of any supporting evidences, we cannot comment on the same.

Although, in general, the heating of the neutrals by collisions with ions cannot be prompt, our observations do not show any appreciable time delay. Further, it is worthwhile to note that such prompt heating over the equatorial thermosphere during the sudden storm commencement (SSC) has also been reported earlier [*Gupta et al*., 1986]. Thus, the present study in tandem with the earlier result shows that our comprehension on the effects of equatorial upper atmosphere, more precisely on the dayglow emissions, associated with the penetration/SSC is far from complete. Therefore, simultaneous space/ground-based measurements along with the modeling studies are called for to better understand the variability of equatorial upper atmosphere, particularly during the transient events of these sorts. Nevertheless, the results which provided strong evidence for the effect of PPEF at equatorial MLTI region are important, and we believe that it can have significant implications in the understanding of the effects of PPEFs over low/equatorial MLTI region. In a complementary point of view, the results also reveal the potential of dayglow spectro/photometry as a unique tool for investigating these space weather effects.

5. Concluding Remarks

The study adduces the effect of penetration events that occurred on 9 April 2006 over the equatorial MLTI region in the Indian longitudes. The ionosonde/magnetometer observations revealed that the equatorial ionosphere responded definitively to PPEFs. The thermospheric OI 630.0 nm dayglow showed a strong depletion associated with the noontime overshielding field. The study revealed that the effect of PPEF is not only restricted to the equatorial ionosphere-thermosphere system but also seen over the mesopause in the form of strong heating (~30 K) as evidenced by ground/space-based measurements. This heating created (a) a reduction in Cowling conductivity over the equator as inferred using magnetometer observations and (b) unusual quenching of $O(^1D)$ atoms at the dayglow emission altitudes as measured using MWDPM. In the authors' view, such studies dealing with the concomitant variations originating from solar wind, interplanetary medium, and equatorial ionosphere/thermosphere extending down to mesosphere are very important to get a comprehensive understanding of solar-terrestrial coupling, particularly during geomagnetically disturbed periods.

Acknowledgments

This work was supported by Department of Space, Government of India. One of the authors, S.G.S. gratefully acknowledges the financial assistance provided by the Indian Space Research Organization (ISRO). The data from MWDPM and ionosonde used in the present analysis, being the property of ISRO, are not available in the public domain due to the organizational restrictions. Authors are thankful to the Director, Indian Institute of Geomagnetism, for providing the magnetic field data, which are available at http://wdc.kugi.kyoto-u.ac.jp/mdplt/index.html. We also acknowledge the use of SABER data from http://saber.gats-inc.com/data.php and interplanetary data from the OMNI Web resource at http://omniweb.gsfc.nasa.gov/. Discussions with M.C. Kelley and J.P. St. Maurice are duly acknowledged.

Michael Liemohn thanks the reviewers for their assistance in evaluating this paper.

References

Balan, N., S. V. Thampi, K. Lynn, Y. Otsuka, H. Alleyne, S. Watanabe, M. A. Abdu, and B. G. Fejer (2008), F_3 layer during penetration electric field, *J. Geophys. Res.*, *113*, A00A07, doi:10.1029/2008JA013206.

Fejer, B. G., R. W. Spiro, R. A. Wolf, and J. C. Foster (1990), Latitudinal variations of penetration electric fields during magnetically disturbed periods: 1986 SUNDIAL observations and model results, *Ann. Geophys.*, *8*, 441–454.

Fejer, B. G., J. W. Jensen, T. Kikuchi, M. A. Abdu, and J. L. Chau (2007), Equatorial ionospheric electric fields during the November 2004 magnetic storm, *J. Geophys. Res.*, *112*, A10304, doi:10.1029/2007JA012376.

Goldberg, R. A., D. N. Baker, F. A. Herrero, S. P. McCarthy, P. A. Twigg, C. L. Croskey, and L. C. Hale (1994), Energy deposition and middle atmosphere electrodynamic response to a highly relativistic electron precipitation event, *J. Geophys. Res.*, *99*, 21,071–21,081, doi:10.1029/94JD00084.

Gupta, R., J. N. Desai, R. Raghava, R. Sekar, R. Sridharan, and R. R. Narayanan (1986), Excess heating over the equatorial latitudes during storm sudden commencement, *Geophys. Res. Lett.*, *13*, 1055–1058, doi:10.1029/GL013i010p01055.

Huang, C.-S., J. C. Foster, and M. C. Kelley (2005), Long-duration penetration of the interplanetary electric field to the low-latitude ionosphere during the main phase of magnetic storms, *J. Geophys. Res.*, *110*, A11309, doi:10.1029/2005JA011202.

Kikuchi, T., Y. Ebihara, K. K. Hashimoto, R. Kataoka, T. Hori, S. Watari, and N. Nishitani (2010), Penetration of the convection and overshielding electric fields to the equatorial ionosphere during a quasiperiodic DP 2 geomagnetic fluctuation event, *J. Geophys. Res.*, *115*, A05209, doi:10.1029/2008JA013948.

Kikuchi, T., K. K. Hashimoto, A. Shinbori, Y. Tsuji, and S. Watari (2011), Penetration of magnetospheric electric fields to the low latitude ionosphere during storm/substorms, in *Aeronomy of the Earth's Atmosphere and Ionosphere*, *IAGA Special Sopron Book Series*, vol. 2, edited by M. A. Abdu, D. Pancheva, and A. Bhattacharyya, pp. 443–453, Springer Science, Heidelberg, Germany.

Krassovsky, V. I. (1972), Infrasonic variations of OH emission in the upper atmosphere, *Ann. Geophys.*, *28*, 739.

Manoj, C., S. Maus, H. Luehr, and P. Alken (2008), Penetration characteristics of the interplanetary electric field to the daytime equatorial ionosphere, *J. Geophys. Res.*, *113*, A12310, doi:10.1029/2008JA013381.

Meriwether, J. W. (1975), High latitude airglow observations of correlated short-term fluctuations in the hydroxyl Meinel 8-3 band intensity and rotational temperature, *Planet. Space Sci.*, *23*, 1211–1221.

Nishida, A. (1968), Coherence of geomagnetic DP2 magnetic fluctuations with interplanetary magnetic variations, *J. Geophys. Res.*, *73*, 5549–5559, doi:10.1029/JA073i017p05549.

Pant, T. K., D. Tiwari, C. Vineeth, S. V. Thampi, S. Sridharan, C. V. Devasia, R. Sridharan, S. Gurubaran, and R. Sekar (2007), Investigation on the mesopause energetics and its possible implications on the equatorial MLTI processes through coordinated daytime airglow and radar measurements, *Geophys. Res. Lett.*, *34*, L15102, doi:10.1029/2007GL030193.

Richmond, A. D., C. Peymirat, and R. G. Roble (2003), Long-lasting disturbances in the equatorial ionospheric electric field simulated with a coupled magnetosphere-ionosphere-thermosphere model, *J. Geophys. Res.*, *108*(A3), 1118, doi:10.1029/2002JA009758.

Senior, C., and M. Blanc (1984), On the control of magnetospheric convection by the spatial distribution of ionospheric conductivities, *J. Geophys. Res.*, *89*, 261–284, doi:10.1029/JA089iA01p00261.

Simi, K. G., S. V. Thampi, D. Chakrabarty, B. M. Pathan, S. R. P. Nayar, and T. K. Pant (2012), Extreme changes in the equatorial electrojet under the influence of interplanetary electric field and the associated modification in the low-latitude F-region plasma distribution, *J. Geophys. Res.*, *117*, A03331, doi:10.1029/2011JA017328.

Solomon, S. C., and V. Abreu (1989), The 630 nm dayglow, *J. Geophys. Res.*, *94*, 6817–6824, doi:10.1029/JA094iA06p06817.

Sreeja, V., T. K. Pant, L. Jose, and S. Ravindran (2011), Westward electric field penetration to the dayside equatorial ionosphere during the main phase of the geomagnetic storm on 22 July 2009, *J. Geophys. Res.*, *116*, A03303, doi:10.1029/2010JA016013.

Sridharan, R., S. A. Haider, S. Gurubaran, R. Sekar, and R. Narayanan (1992), OI 630.0 nm dayglow in the region of equatorial ionization anomaly: Temporal variability and its causative mechanism, *J. Geophys. Res.*, *97*, 13,715–13,721, doi:10.1029/92JA00674.

Sridharan, R., N. K. Modi, D. Pallam Raju, R. Narayanan, T. K. Pant, A. Taori, and D. Chakrabarty (1998), A multiwavelength daytime photometer: A new tool for the investigation of atmospheric processes, *Meas. Sci. Tech.*, *9*, 585.

Sridharan, R., A. Taori, S. Gurubaran, R. Rajaram, and M. G. Shepherd (1999), First results on daytime mesopause OH rotational temperatures using ground-based photometry from equatorial latitudes, *J. Atmos. Sol. Terr. Phys.*, *61*(15), 1131–1142.

Sumod, S. G., T. K. Pant, C. Vineeth, and M. M. Hossain (2011a), A new insight into the vertical neutral-ion coupling between the mesopause and ionosphere F region, *Ann. Geophys.*, *29*, 421–426.

Sumod, S. G., T. K. Pant, C. Vineeth, M. M. Hossain, and M. Antonita (2011b), Response of the tropical mesopause to the longest annular solar eclipse of this millennium, *J. Geophys. Res.*, *116*, A06317, doi:10.1029/2010JA016326.

Sumod, S. G., T. K. Pant, L. Jose, M. M. Hossain, and K. K. Kumar (2012), Signatures of Sudden stratospheric warming on equatorial thermosphere-ionosphere system, *Planet. Space Sci.*, *63–64*, 49–55, doi:10.1016/j.pss.2011.08.005.

Sumod, S. G., T. K. Pant, C. Vineeth, and M. M. Hossain (2014), On the ionospheric and thermospheric response of solar flare events of 19 January 2005: An investigation using radio and optical techniques, *J. Geophys. Res. Space Physics*, *119*, 5049–5059, doi:10.1002/2013JA019714.

Vineeth, C., T. K. Pant, C. V. Devasia, and R. Sridharan (2007), Highly localized cooling in daytime mesopause temperature over the dip equator during counter electrojet events: First results, *Geophys. Res. Lett.*, *34*, L14101, doi:10.1029/2007GL030298.

Xu, J., A. K. Smith, W. Yuan, H.-L. Liu, Q. Wu, M. G. Mlynczak, and J. M. Russell III (2007), Global structure and long-term variations of zonal mean temperature observed by TIMED/SABER, *J. Geophys. Res.*, *112*, D24106, doi:10.1029/2007JD008546.

Zhang, S. P., and G. G. Shepherd (2004), Solar influence on the O (^1D) dayglow emission rate: Global-scale measurements by WINDII on UARS, *Geophys. Res. Lett.*, *31*, L07804, doi:10.1029/2004GL019447.